**Preprints of the 21st IFAC World Congress (Virtual)**
**Berlin, Germany, July 12-17, 2020**

# Actuator Fault Tolerant Control of Variable Pitch Quadrotor Vehicles

**Alessandro Baldini** * **Riccardo Felicetti** * **Alessandro Freddi** *
**Sauro Longhi** * **Andrea Monteriù** *

* *Department of Information Engineering, Università Politecnica delle Marche, Via Brecce Bianche, 60131 Ancona, Italy*
*(e-mail: {a.baldini, r.felicetti}@pm.univpm.it,*
*{a.freddi, sauro.longhi, a.monteriu}@univpm.it)*

**Abstract:** Variable pitch quadrotors can experience actuation faults and failures of two main types: one type related to the rotor system and the other one related to the blade pitch servo. In this paper, we face the fault tolerant attitude tracking problem for a variable pitch quadrotor, in case of partial loss of effectiveness of the rotor system or lock-in-place of the blade pitch servo. The proposed solution is based on the combination of the Disturbance Observer Based Control design paradigm together with that of Active Fault Diagnosis. In detail, an observer is designed for estimating the thrust produced by each rotor. An active diagnosis scheme is adopted to discriminate which fault/failure is affecting the system. Finally, a control allocation algorithm solves the optimal redistribution problem of the control effort among the rotors, subject to different constraints. The proposed overall optimal fault tolerant control scheme can be coupled with most of the nonlinear control laws commonly applied to conventional, fixed pitch, quadrotor systems. Numerical simulations show the capability of the proposed scheme to handle both loss of effectiveness of the rotor system or lock-in-place of the blade pitch servo.

*Keywords:* UAVs; Fault detection and diagnosis; Fault accommodation and Reconfiguration strategies; Active Fault Diagnosis; Applications of FDI and FTC.

## 1. INTRODUCTION

The most common multirotor configuration, namely the quadrotor, is equipped with four fixed pitch blades connected to a motor, controlled by an independent Electronic Speed Controller (ESC). Variable Pitch (VP) quadrotors, instead, can vary both the rotation speed of each motor and the blade pitch of each propeller, resulting in relevant advantages w.r.t. Fixed Pitch (FP) quadrotors: they possess higher thrust rate of change, reverse thrust, allow reverse flight capabilities, and scale well with size (Cutler et al., 2011; Cutler and How, 2012; Gupta et al., 2016).

From a control point of view, both FP and VP quadrotors have similar dynamics, making it possible to easily adapt control laws designed for FP quadrotors to the VP ones. The main difference, instead, lies at the control allocation level, since the pitch of each propeller can be varied: this results in additional degrees of freedom for the allocation, which can be exploited to satisfy additional constraints such as minimizing energy consumption, handling the presence of faults and failures, etc.

The control allocation strictly depends on the model of the thrust provided by each rotating propeller (Pretorius and Boje, 2014; Fresk and Nikolakopoulos, 2014; Cutler and How, 2015; Gupta et al., 2016; Arellano-Quintana et al., 2018), and two main alternatives are proposed in the literature. The simpler one is to assume constant motor speeds and use pitch angles as sole control inputs, as proposed in Cutler et al. (2011); Pretorius and Boje (2014); Gupta et al. (2016); Pang et al. (2016). A less common (and more complex) alternative is to exploit both pitch angles and motor speeds to produce the desired thrust, as done in Sheng and Sun (2016); Arellano-Quintana et al. (2018) (and, partially, in Fresk and Nikolakopoulos (2014); Porter et al. (2016)). The latter alternative is harder to solve online, due to its inherent nonlinearity, but at the same time it provides input redundancy which is necessary to provide actuator fault tolerance while satisfying actuation constraints.

By the way, none of the previous works deal with actuator faults or failures in VP quadrotors. Actuation fault/failures in this kind of vehicles are mainly of two types: they may affect the rotor system (ESC, motor, and propeller) or the blade pitch servo. As for the rotor system, the most common fault consists in a Loss Of Effectiveness (LOE), i.e., the produced thrust is reduced with respect to the commanded/desired one, eventually degenerating into a failure when the thrust is zero. LOE has many causes: battery voltage affects thrust (Podhradskỳ et al., 2013), pitch increase may slow down motor speed due to increased drag (Cutler and How, 2015), and finally any physical damage to the rotor system should also be considered. As for the pitch servo instead, lock-in-place is a common failure in electromechanical servo actuators (Qiao et al., 2018), namely the blade pitch becomes stuck and can not be changed anymore.

In this paper, we propose a Fault Tolerant Control (FTC) scheme to solve the attitude tracking problem for a VP

quadrotor. The scheme can deal with both rotor system faults and lock-in-place failures, while taking into account both actuator saturation and rate limits. In detail, assuming accessible state, a nonlinear observer is developed to detect thrust anomalies. When an anomaly is detected, an active diagnosis strategy is adopted to discern between LOE or lock-in-place, and provides the estimation accordingly. The control allocation algorithm exploits such information and distributes the control efforts among the actuators, commanding both blade pitches and motor speeds in case of LOE (accommodation policy), while modifying the motor speed only for the corresponding locked-in-place pitch servo (reconfiguration policy).

The paper is structured as follows. The mathematical model of the quadrotor is shortly introduced in Section 2. Section 3 is devoted to the design of the control scheme. In Section 4, the fault detection, isolation, and estimation algorithms are detailed. Numerical simulations are presented in Section 5 and conclusions end the paper.

## 2. SYSTEM MODEL

The mathematical model of VP drones is not so different from its FP counterpart: the only difference is the way forces and moments are generated. We follow a Newton-Euler approach, as we have done in the previous work Lanzon et al. (2014) regarding FP drones, where we have considered an earth fixed frame $O_E - \{x_E, y_E, z_E\}$ and a body fixed frame $O_B - \{x_B, y_B, z_B\}$, together with a roll, pitch, yaw convention. Let $\varphi$, $\theta$, and $\psi$ be the roll, pitch, and yaw angles, let $p$, $q$, and $r$ be the rotational speeds along the axes of $O_B$, let $z$ be the $z_E$ component of the center of mass position in the earth frame and $g$ the gravitational acceleration (see Fig. 1(a)). We denote with $\tau_p$, $\tau_q$, and $\tau_r$ the generalized torques provided by the actuators, and we define the artificial variables $u_p = \tau_p/l$, $u_q = \tau_q/l$, and $u_r = \tau_r$. Moreover, we denote with $u_f$ the upward lift force produced by the actuators, and acting on the center of mass. Neglecting the gyroscopic effect, the following model describes the attitude and altitude dynamics of a generic multirotor drone (please refer to Table 1 for the meaning of each parameter):

$$\begin{aligned} I_x\dot{p} &= -qr(I_z - I_y) - k_{rp}p + lu_p \\ I_y\dot{q} &= -pr(I_x - I_z) - k_{rq}q + lu_q \\ I_z\dot{r} &= -pq(I_y - I_x) - k_{rr}r + u_r \\ \dot{\varphi} &= p + q\sin(\varphi)\tan(\theta) + r\cos(\varphi)\tan(\theta) \\ \dot{\theta} &= q\cos(\varphi) - r\sin(\varphi) \\ \dot{\psi} &= (q\sin(\varphi) + r\cos(\varphi))/\cos(\theta) \\ m\ddot{z} &= -cos(\varphi)\cos(\theta)u_f - k_t\dot{z} + mg \end{aligned} \tag{1}$$

The vector $u = [u_f \ u_p \ u_q \ u_r]^T$ represents the generalized virtual inputs for the system, namely the control forces/torques we want to generate in order to fly the system. The way how these forces/torques are then effectively generated is related to the rotors configuration.

### 2.1 Input mapping

Let us consider the case of rectangular, untwisted blades with uniform inflow. As long as the propeller is not stalling, the thrust $T_i$ and the torque $Q_i$ of each rotor,

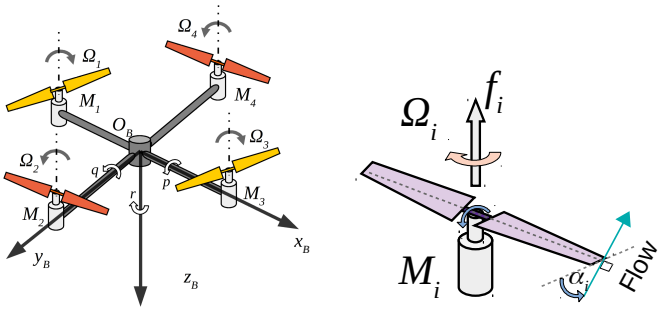


(a) Body frame (b) Variable pitch thruster

Fig. 1. Variable pitch quadrotor.

$i = 1, \dots 4$, can be expressed as a function of thrust coefficient and rotational speed using blade element theory and momentum theory (Gupta et al., 2016):

$$T_i = (C_{T_i}(\alpha_i)\rho\pi R^4)w_i^2\omega_i^2 \doteq c_L(\alpha_i)w_i^2\omega_i^2 \tag{2}$$

$$Q_i = (C_{Q_i}(\alpha_i)\rho\pi R^5)w_i^2\omega_i^2 \doteq c_D(\alpha_i)w_i^2\omega_i^2 \tag{3}$$

where $\omega_i > 0$ is the rotational speed of the $i$-th motor, $w_i$ are additional (unknown, nominally equal to 1) parameters that take into account potential thrust loss effects (as it will be discussed in the following section), and $c_L(\alpha_i), c_D(\alpha_i)$ are the lift and drag coefficients. $C_{T_i}(\alpha_i)$ and $C_{Q_i}(\alpha_i)$ are dimensionless thrust and torque coefficients: assuming steady, linearized blade aerodynamics (see Leishman (2006) for further details), they nonlinearly depend on the pitch angle $\alpha_i$ as follows:

$$\alpha_i = \frac{6C_{T_i}}{\sigma C_{l\alpha_i}} + \frac{3}{2}\sqrt{\frac{C_{T_i}}{2}} \tag{4}$$

$$C_{Q_i} = \frac{C_{T_i}^{3/2}}{\sqrt{2}} + \frac{1}{8}\sigma C_{d0_i} \tag{5}$$

As rectangular untwisted blades are symmetric, the equations (4) and (5) in Leishman (2006) can be extended to the case of negative pitch angles, obtaining a negative lift coefficient because the thrust changes direction, while the drag coefficient remains positive because it counteracts the propeller rotation. In particular, the resulting $C_{T_i}(\alpha_i)$ is an odd function of $\alpha_i$, while $C_{Q_i}(\alpha_i)$ becomes an even function of $\alpha_i$. Also note that it is not possible to obtain an explicit function $C_{T_i}(\alpha_i)$ from (4) in terms of elementary functions. We assume that the pitch angles $\alpha_i$ and the motor speeds $\omega_i$ represent control variables (see Fig. 1(b)), where the former are commanded via pitch servo-actuators and the latter are commanded by means of ESCs. The system is inherently overactuated: for each given control command $u$, more than one combination of control variables $\alpha_i, \omega_i$ that produce such effort exist. The input mapping is finally given by

$$\begin{aligned} u_f = \ & c_L(\alpha_1)w_1^2\omega_1^2 + c_L(\alpha_2)w_2^2\omega_2^2 \\ & + c_L(\alpha_3)w_3^2\omega_3^2 + c_L(\alpha_4)w_4^2\omega_4^2 \\ u_p = \ & -c_L(\alpha_2)w_2^2\omega_2^2 + c_L(\alpha_4)w_4^2\omega_4^2 \\ u_q = \ & -c_L(\alpha_1)w_1^2\omega_1^2 + c_L(\alpha_3)w_3^2\omega_3^2 \\ u_r = \ & -c_D(\alpha_1)w_1^2\omega_1^2 + c_D(\alpha_2)w_2^2\omega_2^2 \\ & - c_D(\alpha_3)w_3^2\omega_3^2 + c_D(\alpha_4)w_4^2\omega_4^2 \end{aligned} \tag{6}$$

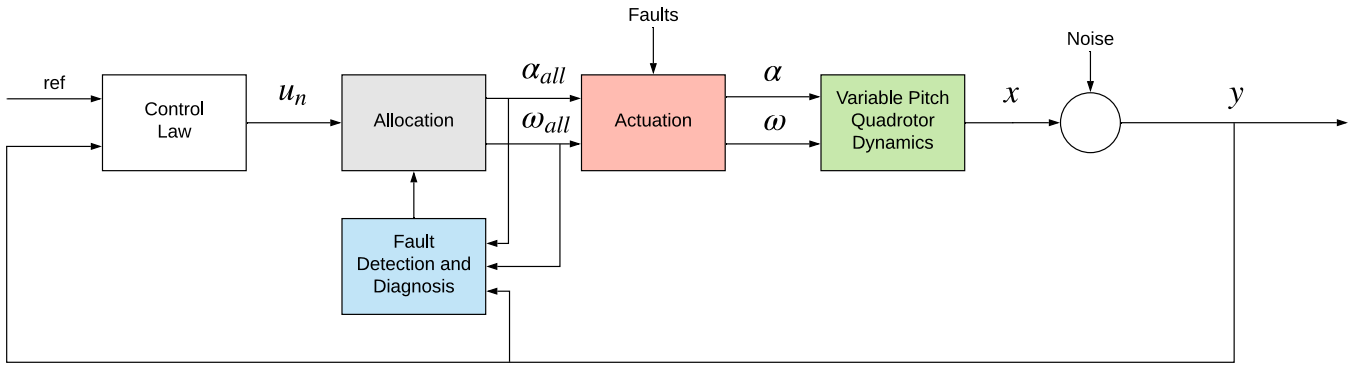


Fig. 2. Overview of the control scheme.

### 2.2 Actuator dynamics and faults

Both the motor and the pitch servo have fast dynamics if compared with the vehicle dynamics, hence they can be modeled with simple saturations and rate limits, as done in Cutler et al. (2011). Two major actuator faults/failures may occur:

- servo-actuator failure: the pitch angle becomes unresponsive (lock-in-place);
- rotor fault: the produced thrust is lower than expected ($w_i < 1$, LOE, e.g., the actual motor speed may differ from the commanded one).

As we independently control pitch and speed of each actuator, both issues can be overcome effectively in many cases, provided that the fault and/or failure are diagnosed in short time. On the contrary, in case of rotor complete failure (or, similarly, stuck pitch in feathered position), there is no further actuator redundancy to be exploited (Mancini et al., 2007; Baldini et al., 2019a) and the quadrotor vehicle becomes underactuated: the tracking task cannot be performed anymore, hence different strategies must be adopted to safely land the vehicle (Lanzon et al., 2014).

## 3. CONTROL ALLOCATION

The overall control scheme is reported in Fig. 2. Assuming the reference is provided, any (nonlinear) control law giving $u_n$, namely the nominal generalized control forces/torques, is suitable for this scheme, because accommodation and reconfiguration are performed by the control allocation algorithm. The actuator faults and the vehicle dynamics have been already discussed in Section 2, while the Fault Detection and Diagnosis (FDD) module will be discussed in the Section 4.

The proposed solution avoids nonlinear programming algorithms, which may result slow, and relies on reasonable approximations to make the problem linear. Let us define $\check{c}_L(\alpha_i)$ and $\check{c}_D(\alpha_i)$ as polynomial functions (fourth and second order, respectively) that approximate $c_L(\alpha_i)$ and $c_D(\alpha_i)$ respectively, that is to say the inverse of (4), (5). There, the approximation error in $|\alpha_i| > 3°$ is up to 1.7% for the lift and up to 4.3% for the drag coefficient (see Fig.3). We rewrite (6) as $u = BT$, namely:

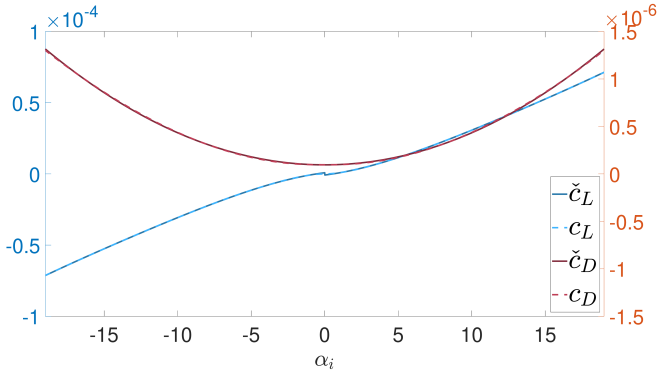


Fig. 3. Lift and drag coefficients, polynomial approximations.

$$\begin{bmatrix} u_f \\ u_p \\ u_q \\ u_r \end{bmatrix} = \begin{bmatrix} 1 & 1 & 1 & 1 \\ 0 & -1 & 0 & 1 \\ -1 & 0 & 1 & 0 \\ -c_D/c_L & c_D/c_L & -c_D/c_L & c_D/c_L \end{bmatrix} \begin{bmatrix} T_1 \\ T_2 \\ T_3 \\ T_4 \end{bmatrix} \tag{7}$$

where $T = [T_1\ T_2\ T_3\ T_4]^T$ are the upward lift forces defined in (2). The relation is still nonlinear, because the allocation matrix is input-dependent, but we also note that $c_D(\alpha_i)/c_L(\alpha_i)$ is almost constant when $\alpha_i$ is sufficiently distant from zero ($|\alpha_i| > 3°$), which is true in the most effective pitch configurations: in fact, small pitch angles involve very low lift forces and thus they are avoided in most of the flight time. Hence we approximate $c_D(\alpha_i)/c_L(\alpha_i)$ with $\check{c}_D(\hat{\alpha}_i)/\check{c}_L(\hat{\alpha}_i)$, where $\hat{\alpha}_i$ is the blade pitch estimated by the FDD module, resulting in the locally approximated allocation matrix $\check{B}$, which is numerical. We rewrite (7) in the Quadratic Programming (QP) framework considering the energy-like cost function and constraints:

$$\begin{aligned} &\min_T \ \|T\|^2 \\ &s.t.\ \ \check{B}T = u_n \\ &\qquad T_{i_{\min}} \le T_i \le T_{i_{\max}} \quad (\forall i = 1, \dots, 4) \end{aligned} \tag{8}$$

where $T_{i_{\min}}$ and $T_{i_{\max}}$ are calculated at each step as:

$$\begin{aligned} T_{i_{\min}} &= \begin{cases} \check{c}_L(\alpha_{i_{min}})\hat{w}_i^2\omega_{i_{min}}^2 & \text{if } \check{c}_L(\alpha_{i_{min}}) \ge 0 \\ \check{c}_L(\alpha_{i_{min}})\hat{w}_i^2\omega_{i_{max}}^2 & \text{if } \check{c}_L(\alpha_{i_{min}}) < 0 \end{cases} \\ T_{i_{\max}} &= \begin{cases} \check{c}_L(\alpha_{i_{max}})\hat{w}_i^2\omega_{i_{max}}^2 & \text{if } \check{c}_L(\alpha_{i_{max}}) \ge 0 \\ \check{c}_L(\alpha_{i_{max}})\hat{w}_i^2\omega_{i_{min}}^2 & \text{if } \check{c}_L(\alpha_{i_{max}}) < 0 \end{cases} \end{aligned} \tag{9}$$

and the bounds of $\alpha_i$ and $\omega_i$ are given by the constraints:

$$\begin{array}{rcl} \alpha_{i_{min}} & = & \max\ (\ \alpha_{min}\ ,\ \hat{\alpha}_i - \kappa_i d_{\alpha_i}\ ) \\ \alpha_{i_{max}} & = & \min\ (\ \alpha_{max}\ ,\ \hat{\alpha}_i + \kappa_i d_{\alpha_i}\ ) \\ \omega_{i_{min}} & = & \max\ (\ 0\ \ ,\ \omega_{i_{pr}} - d_{\omega_i}\ ) \\ \omega_{i_{max}} & = & \min\ (\ \omega_{max}\ ,\ \omega_{i_{pr}} + d_{\omega_i}\ ) \end{array} \tag{10}$$

Note that the bounds $T_{i_{min}}$ and $T_{i_{max}}$ depend on the current pitch angles. This makes possible to consider constraints on both the instantaneous values of $T_i$ and its rate. Moreover, $\hat{w}_i$ is the rotor system LOE estimated by the FDD module, $\alpha_{min}, \alpha_{max}, 0, \omega_{max}$ model the actuator saturation, $d_{\alpha_i}, d_{\omega_i}$ model the maximum variation in one allocation step (in nominal conditions), $\kappa_i \in \{0, 1\}$ is employed to lock the pitch angle when necessary (reconfiguration), and $\omega_{i_{pr}}$ represents the solution of the previous allocation step. We solve the constrained QP problem with the weighted least squares method (Harkegard, 2002) because of its short computation time and its capability to cope with feasible and unfeasible constrained problems. It solves the following relaxed problem with an active set method:

$$\begin{array}{l} T_{all} = \arg\min_{T}[\ \|T\|^2 + \gamma\|\Xi(\check{B}T - u_n)\|^2] \\ \qquad s.t.\ T_{i_{\min}} \leq T_i \leq T_{i_{\max}} \quad (\forall i = 1, \ldots, 4) \end{array} \tag{11}$$

where $\gamma = 10^6$ prioritizes the constraint $\check{B}T = u_n$ and $\Xi = \mathrm{diag}([1, 1, 1, 100])$ is a weighting matrix to cope with the unbalanced values in the rows of $\check{B}$.
Once $T_{all}$ is obtained, it is necessary to find the couples $(\alpha_{all_i}, \omega_{all_i})$ such that $T_{all_i} = \check{c}_L(\alpha_{all_i})\hat{w}_i^2\omega_{all_i}^2 (\forall i = 1, \ldots, 4)$, which is certainly possible because $T_{all}$ satisfies the box constraint in (11). Among the possible solutions, we prefer to keep the motor speed as constant as possible, because the pitch angle is more responsive (Cutler and How, 2015), and to vary motor speed only when the pitch alone is not sufficient to obtain the desired thrusts.

## 4. FAULT DIAGNOSIS AND ACCOMMODATION

The fault diagnosis problem consists in estimating both the LOE of the rotor system $w_i$ and the blade pitch $\alpha_i$, as well as providing the index of the eventually stuck pitch servo. The problem can be solved (see Fig. 4) given the knowledge of:

- the allocated pitch angles $\alpha_{all}$
- the allocated motor speeds $\omega_{all}$
- the measure $y$ of the state variables

where for allocated we mean the output of the allocation algorithm (also see Fig. 2). Since the problem requires the determination of eight independent variables (estimation of $\alpha$ and $\omega$) which affect only the last four equations of (1), the problem cannot be solved without additional knowledge (e.g., measuring jerk), thus we propose the policy described in the following. First of all, we recover the allocated forces $T_{all}$ and the allocated generalized inputs $u_{all} = \begin{bmatrix} u_{all_f} & u_{all_p} & u_{all_q} & u_{all_r} \end{bmatrix}^T$:

$$T_{all_i} = \check{c}_L(\alpha_{all_i})\hat{w}_i^2\omega_{all_i}^2 \quad (i = 1, \ldots, 4) \tag{12}$$

$$u_{all} = \check{B}T_{all} \tag{13}$$

We remark that $u_{all}$ may differ from $u_n$ for two reasons: the allocation performs some approximation, and the effort $u_n$ may be infeasible due to the constraints.

### 4.1 Input observer

The allocated input $u_{all}$ can be substantially different from the actual input $u$ acting on the vehicle, because of the presence of actuator faults. The following input observer provides an estimation of this difference, namely $\Delta u = u - u_{all}$, which is bounded if we neglect the presence of measurement noise and we assume $u_{all}$ and $\dot{u}_{all}$ are bounded as well. Such boundedness conditions also ensures that $\left\|\dot{\Delta u}\right\| \leq \rho$ for some $\rho > 0$.

Let us define $\eta_1 = [z\ \varphi\ \theta\ \psi]^T$ and $\eta_2 = [\dot{z}\ p\ q\ r]^T$, so that model (1) can be rewritten in the form

$$\dot{\eta}_1 = \gamma_1(\eta_1, \eta_2) \tag{14}$$

$$\dot{\eta}_2 = \gamma_2(\eta_2) + \Gamma(\eta_1)u_{all} + \Gamma(\eta_1)\Delta u \tag{15}$$

where $\gamma_1$ and $\gamma_2$ are four dimensional vectors, $\Gamma$ is a square matrix of order four and all of their entries are smooth with respect to the denoted variables. Moreover, $\Gamma(\eta_1)$ is invertible for $-\frac{\pi}{2} < \varphi, \theta < +\frac{\pi}{2}$.

We define the variable

$$s = -\lambda(\eta_1, \eta_2) + \Delta u \tag{16}$$

where $\lambda(\cdot, \cdot)$ is a continuously differentiable function to choose. We can show that, after some manipulation (following the DOBC framework as in Chen et al. (2016)), the dynamics of $s$ is

$$\dot{s} = -\frac{\partial\lambda(\eta_1, \eta_2)}{\partial\eta_2}\Gamma(\eta_1)s + R(\eta_1, \eta_2, u_{all}) + \dot{\Delta u} \tag{17}$$

where

$$\begin{aligned} R(\eta_1, \eta_2, u_{all}) = & -\frac{\partial\lambda(\eta_1, \eta_2)}{\partial\eta_1}\gamma_1(\eta_1, \eta_2) \\ & - \frac{\partial\lambda(\eta_1, \eta_2)}{\partial\eta_2}\left[\gamma_2(\eta_2) + \Gamma(\eta_1)(\lambda(\eta_1, \eta_2) + u_{all})\right] \end{aligned}$$

is a function of known variables. We can find an observer in the form

$$\dot{\hat{s}} = -\frac{\partial\lambda(\eta_1, \eta_2)}{\partial\eta_2}\Gamma(\eta_1)\hat{s} + R(\eta_1, \eta_2, u_{all}) \tag{18}$$

$$\widehat{\Delta u} = \hat{s} + \lambda(\eta_1, \eta_2) \tag{19}$$

The dynamics of the observation error $\tilde{s} = s - \hat{s}$ is described by

$$\dot{\tilde{s}} = -\frac{\partial\lambda(\eta_1, \eta_2)}{\partial\eta_2}\Gamma(\eta_1)\tilde{s} + \dot{\Delta u} \tag{20}$$

which can be made ultimately bounded choosing

$$\lambda(\eta_1, \eta_2) = \Phi(\eta_1)\Gamma(\eta_1)^{-1}\eta_2 \tag{21}$$

where $\Phi(\eta_1) \in \mathbb{R}^{4\times4}$ is any matrix such that

$$\Phi^T(\eta_1)P + P\Phi(\eta_1) \geq \alpha_0 I \qquad \forall\eta_1 \tag{22}$$

for some symmetric positive definite matrix $P \in \mathbb{R}^{4\times4}$ and $\alpha_0 > 0$. Indeed, consider the Lyapunov function $V = \tilde{s}^T P\tilde{s}$, it follows that

$$\begin{aligned} \dot{V} &= -\tilde{s}^T\left[\Phi^T(\eta_1)P + P\Phi(\eta_1)\right]\tilde{s} + 2\tilde{s}^T P\dot{\Delta u} \\ &\leq -\alpha_0\|\tilde{s}\|^2 + 2\rho\|P\|\,\|\tilde{s}\| \end{aligned} \tag{23}$$

which is negative for $\|\tilde{s}\| \geq 2\rho\|P\|/\alpha_0$, and hence $\tilde{s}$ is ultimately bounded. The estimation error $\widetilde{\Delta u} = \Delta u - \widehat{\Delta u}$ is

$$\widetilde{\Delta u} = [s + \lambda(\eta_1, \eta_2)] - [\hat{s} + \lambda(\eta_1, \eta_2)] = s - \hat{s} = \tilde{s} \tag{24}$$

and then $\dot{\widetilde{\Delta u}} = \dot{\tilde{s}}$, thus $\widetilde{\Delta u}$ is ultimately bounded as well. Any constant symmetric positive definite matrix $\Phi(\eta_1)$

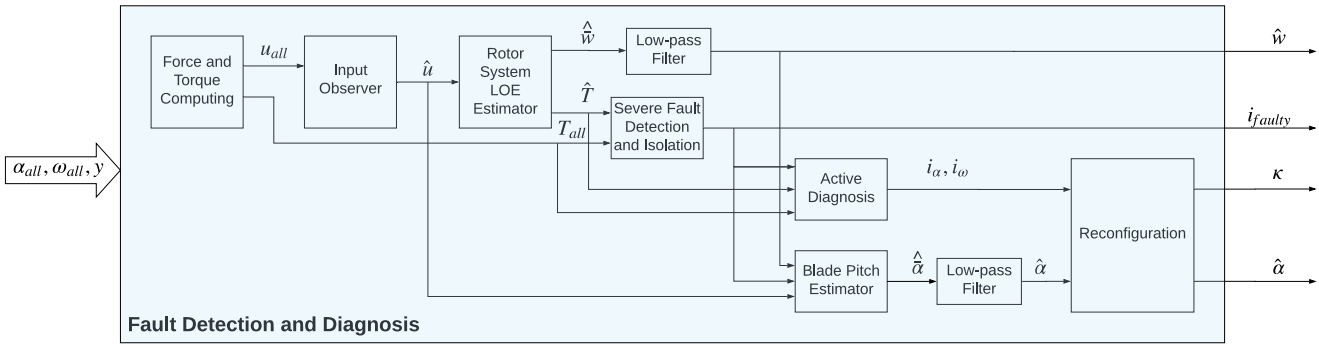


Fig. 4. Detail of the fault detection and diagnosis algorithm.

satisfies (22), hence we impose $\Phi(\eta_1) = k_{obs} I_4$, where $k_{obs} > 0$ is a project parameter.

### *4.2 Loss of effectiveness estimation*

In order to obtain an estimation of the LOE, let us start assuming there are no stuck faults at this stage. From the knowledge of $\hat{u} = u_{all} + \widehat{\Delta u}$, we can estimate the LOE $w_i$ of each actuator, assuming that no servo failures occur (their presence is tackled later). In fact, we can calculate

$$\hat{T} = \check{B}^{-1}\hat{u} \tag{25}$$

$$\hat{\hat{w}}_i = \sqrt{\frac{\hat{T}_i}{\check{c}_L(\alpha_{all_i})\omega_{all_i}^2}} \quad (i = 1, \dots, 4) \tag{26}$$

A single solution always exists, because we know that $\hat{T}_i$ and $\check{c}_L(\alpha_{all_i})$ have the same sign, $\omega_{all_i} > 0$ in any working condition and hence we require $\hat{\hat{w}}_i$ to be positive as well. Finally, it is necessary to low pass filter $\hat{\hat{w}}_i$ to counter the effects of sensor noise: in this way, we obtain the estimation $\hat{w}_i$ of $w_i$, that measures the LOE of each $i$-th actuator. The estimation $\hat{w}_i$ is then fed to the control allocation algorithm, in order to compensate such thrust loss.

### *4.3 Severe fault detection*

The difference between $T_{all}$ and $\hat{T}$ is minimal when $w$ varies slowly, since the allocation algorithm performs an online accommodation exploiting $\hat{w}$. Abrupt variations of $w$, instead, as well as servo failures, make $\hat{T}$ differ significantly from $T_{all}$. As such, the residual $r_d = T_{all} - \hat{T}$ is adopted for severe fault detection. Due to the presence of noise, basic thresholding is not sufficient and we evaluate each scalar residual $r_{d_i}$ $(i = 1, \dots, 4)$, with a Narendra filter (Hecker et al., 2011):

$$\begin{aligned} \dot{\xi}_i &= -\gamma_N \xi_i + \|r_{d_i}\|^2 \\ \theta_i &= \alpha_N \|r_{d_i}\| + \beta_N \sqrt{\xi_i} \end{aligned} \tag{27}$$

where $\alpha_N \geq 0, \beta_N > 0, \gamma_N > 0$ are design parameters to choose according to the measurement noise. The following adaptive threshold $\delta$ is defined:

$$\delta = \delta_N + \sum_{i=1}^{4} \frac{\theta_i}{4} \tag{28}$$

where $\delta_N$ is a constant term depending on the noise amplitude, while the second term accounts for simultaneous variations of each $\theta_i$. When a severe fault occurs, if we assume the probability of simultaneous severe faults to be negligible, then we expect the threshold $\delta$ to be crossed by a single $\theta_i$. When a steep reference change is provided instead, all $\theta_i$ are expected to increase and possibly cross the threshold $\delta$ as the result of inaccurate estimation in fast transients. Using such adaptive method, if $\theta_i < \delta$, then no severe fault is happening (i.e., $i_{faulty} = 0$ in Fig. 4), instead if $\theta_i > \delta$ then the $i$-th actuator is subject to a severe fault (i.e., $i_{faulty} = i$ in Fig. 4) and we need to determine whether this is the consequence of an abrupt LOE or of a servo failure.

### *4.4 Active fault diagnosis*

Once the faulty actuator has been isolated, a feasible strategy to distinguish between pitch servo failure or abrupt rotor fault is necessary. In fact, note that the effects of pitch failure and abrupt LOE on the same actuator are not separable with passive methods, because they share the same input channel. For this reason, an Active Fault Diagnosis (AFD) solution is here adopted, which in general consists in using an auxiliary input signal that is injected into the monitored system in order to improve the quality of decision (Gao et al., 2015; Punčochář and Škach, 2018). The triggering event that starts the procedure is the detection of a severe fault, i.e., $i_{faulty} \neq 0$. Then, the injection is kept for a fixed time length, and the decision is made at the end of the interval. The main concern is to ensure that the active diagnosis does not compromise stability, so we propose the following maneuver, which has no impact at all in absence of faults and failures.
Let us assume the quadrotor is hovering, for the sake of clarity: the $i$-th thruster has to provide an upward force $T_{n,i}$, hence the control allocation generates a couple $(\alpha_{all_i}, \omega_{all_i})$ such that $T_{all_i} = \check{c}_L(\alpha_{all_i})\hat{w}_i^2\omega_{all_i} \approx T_{n,i}$. We suppose an accurate estimation $\hat{w}_i$ of $w_i$ is available and $\alpha_i > 0$ because we are hovering. If we force $\alpha_{all_i}$ to decrease, the allocation increases $\omega_{all_i}$ to prevent $T_{all_i}$ from dropping (as long as saturation and rate limit allows it). In presence of faults, the actual force $T_i$ differs from the allocated one $T_{all_i}$, depending on the nature of the fault:

- if the pitch angle is stuck, $\alpha_i > \alpha_{all_i} \rightarrow T_i > T_{all_i}$;
- if the rotor is faulty, $w_i^2\omega_i^2 < \hat{w}_i^2\omega_{all_i}^2 \rightarrow T_i < T_{all_i}$.

Due to the presence of noise and detection delays, this idea is not usable in this form, moreover we only dispose of the estimation $\hat{T}_i$ of $T_i$. So, the input injection consists in com-

manding the allocation to constrain a strictly decreasing $\alpha_{all_i}$ over time for a fixed time length, and we introduce

$$d_i = \frac{\hat{T}_i - T_{all_i}}{\hat{T}_i} \approx \frac{c_L(\alpha_i) w_i^2 \omega_i^2 - \check{c}_L(\alpha_{all_i}) \hat{w}_i^2 \omega_{all_i}^2}{c_L(\alpha_i) w_i^2 \omega_i^2} \quad (29)$$

It can be shown that an abrupt fault on the rotor system makes $d_i < 0$ as soon as the speed increases; on the contrary, a stuck pitch makes $d_i > 0$ as soon as $\alpha_{all_i} < \alpha_i$, which is not necessarily true when the active detection starts, because $\alpha_{all_i}$ may have increased during the detection delay while $\alpha_i$ was stuck. As a precaution, we freeze the value of $\hat{w}_i$ (for the calculation of $d_i$ only, and eventually for the subsequent stuck estimation) at the beginning of the active diagnosis phase, to prevent it from converging to $w_i$ and thus complicating the diagnosis. Finally, to cope with noise, we use a run-sum test (Isermann, 2006), voting on the basis of the sign of $d_i$, and we weigh more the last samples, because they have a greater chance to satisfy $\alpha_{all_i} < \alpha_i$ in the case of servo failures. The result of the run-sum test, after a fixed time length active diagnosis, is the decision whether the $i$-th rotor is affected by an abrupt fault or the $i$-th pitch angle is locked-in-place. In the first case, no additional action is taken, because the estimation (26) will converge to $w_i$. In the second case, it is also necessary to estimate the stuck pitch angle for a correct allocation of the control effort.

### *4.5 Stuck estimation*

Once the servo failure on actuator $i$ has been isolated, the estimation of $\alpha_i$ is straightforward: it is sufficient to isolate $c_L(\alpha_i)$ from (6), and then to substitute each $w_i^2\omega_i^2$ with $\hat{w}_i^2\omega_{all_i}^2$ and each $c_L(\alpha_j)$, $j \neq i$, with $\check{c}_L(\alpha_{all_j})$. We obtain a system of four linear equations in the only unknown $\alpha_i$: there are no unknowns in one of the equations (the second or the third, depending on $i$), hence such equation can be removed. Moreover, the fourth equation depends on $c_D(\alpha_i)$ while the others depend on $c_L(\alpha_i)$, so the fourth equation is arbitrarily discarded to avoid further approximations.
In conclusion, $c_L(\alpha_i)$ is obtained as the least squares solution of the linear system made of the remaining two equations, and $\hat{\bar{\alpha}}_i$ is consequently calculated using (4). The estimation $\hat{\alpha}_i$ is obtained low pass filtering $\hat{\bar{\alpha}}_i$, to reduce the impact of noise. Finally, the reconfiguration block feeds the information about the current pitch angles to the allocation algorithm, including the status of the pitch servo and, eventually, the estimation of the stuck pitch angle. If the $i$-th servo is not affected by a failure, we set $\hat{\alpha}_i = \alpha_{all_i}$ instead.

## 5. SIMULATION RESULTS

We have tested the control scheme in simulation with a VP quadrotor whose parameters are reported in Table 1. The control law is based on feedback linearization (see, for example, Zhou et al. (2010); Baldini et al. (2019b)); moreover, to increase realism of the simulation, the effectiveness of each motor $w_i$ is supposed to slightly decrease when the respective propeller drag coefficient $c_{D_i}$ increases. Accelerometer and gyroscope additive white gaussian noise is simulated according to the datasheet of the (TDK InvenSense, 2016) MPU-9250 IMU, which is commonly adopted by the commercial Cube autopilot (also known as Pixhawk 2 autopilot). Noise on the remaining state variables is assumed to be one order of magnitude lower due to Kalman filtering.

Table 1. Quadrotor parameters.

| **Parameter** | **Name** | **Value** | **Unit** |
|---|---|---|---|
| Total system mass | $m$ | 1.37 | $[kg]$ |
| Inertia about $x_B$, $y_B$ | $I_x$,$I_y$ | $7.5 \cdot 10^{-3}$ | $[kg \cdot m^2]$ |
| Inertia about $z_B$ | $I_z$ | $1.3 \cdot 10^{-2}$ | $[kg \cdot m^2]$ |
| Arm length | $l$ | 0.3 | $[m]$ |
| Lift curve slope | $c_{l_\alpha}$ | 5.23 | $[-]$ |
| Zero lift drag coefficient | $c_{d_0}$ | 0.01 | $[-]$ |
| Propeller radius | $R$ | 0.18 | $[m]$ |
| Propeller chord | $c$ | 0.03 | $[m]$ |
| Rotor solidity | $\sigma$ | 0.106 | $[-]$ |
| Gravitational acceleration | $g$ | 9.81 | $[m/s^2]$ |
| Air density | $\rho$ | 1.225 | $[kg/m^3]$ |
| Linear friction coefficient | $k_t$ | $4.8 \cdot 10^{-2}$ | $[N \cdot s/m]$ |
| Roll friction coefficient | $k_{rp}$ | $5.6 \cdot 10^{-4}$ | $[N \cdot s \cdot m]$ |
| Pitch friction coefficient | $k_{rq}$ | $5.6 \cdot 10^{-4}$ | $[N \cdot s \cdot m]$ |
| Yaw friction coefficient | $k_{rr}$ | $5.6 \cdot 10^{-4}$ | $[N \cdot s \cdot m]$ |
| Minimum pitch angle | $\alpha_{min}$ | $-19$ | $[deg]$ |
| Maximum pitch angle | $\alpha_{max}$ | 19 | $[deg]$ |
| Pitch angle rate limit | $d_{\alpha_i}$ | 630 | $[deg/s]$ |
| Maximum motor speed | $\omega_{max}$ | 339 | $[rad/s]$ |
| Motor speed rate limit | $d_{\omega_i}$ | 7330 | $[rad/s^2]$ |

### *5.1 Single flight*

We propose a simulation where three faults occur. In particular, actuator 2 experiences a gradual LOE at $t = 5$s, servo 3 fails (i.e. lock-in-place) at $t = 10$ s and actuator 4 is subject to an abrupt LOE at $t = 15$ s (see Figs. (6)-(7)). The reference trajectory and the tracking performances are reported in Fig. 5. The first fault is not sufficiently abrupt to make the residual overcome the threshold (see Fig. 8), so no AFD is triggered and a simple accommodation thanks to $\hat{w}_i$ (Fig. 7) is performed, and the commanded motor speed is increased consequently. The tracking performances temporarily decrease, see in particular $\varphi$ in Fig. 5. The second fault is detected after 274 ms: the AFD ends after additional 50 ms, it isolates the failure in servo 3 (stuck) and commands control reconfiguration, thus avoiding to use $\alpha_{all_3}$ as a control variable. The pitch estimation error is less than 0.6deg, and the LOE estimation shows an offset that partially compensates for the pitch estimation error. The tracking performances do not show significant variations in this time interval. Finally, the third fault is detected after 96 ms: the AFD isolates a LOE in rotor 4, so no reconfiguration is performed. A transient performance deterioration occurs until the LOE estimation $\hat{w}_4$ settles to the right value.

### *5.2 Error analysis*

We have performed 100 simulations with the same reference of the previous scenario, injecting in each test only one severe LOE or servo failure. In 50 simulations, a random servo fails at $t \in [1, 15]s$; in the remaining simulations, a random rotor is affected by a LOE which starts at $t \in [1, 15]s$ and decreases to $w_i \in [0.8, 0.95]$ after $\Delta t \in [0.1, 0.5]s$. The random variables are independently uniformly distributed in their interval. The results are resumed in Table 2, which reports the success rates, namely

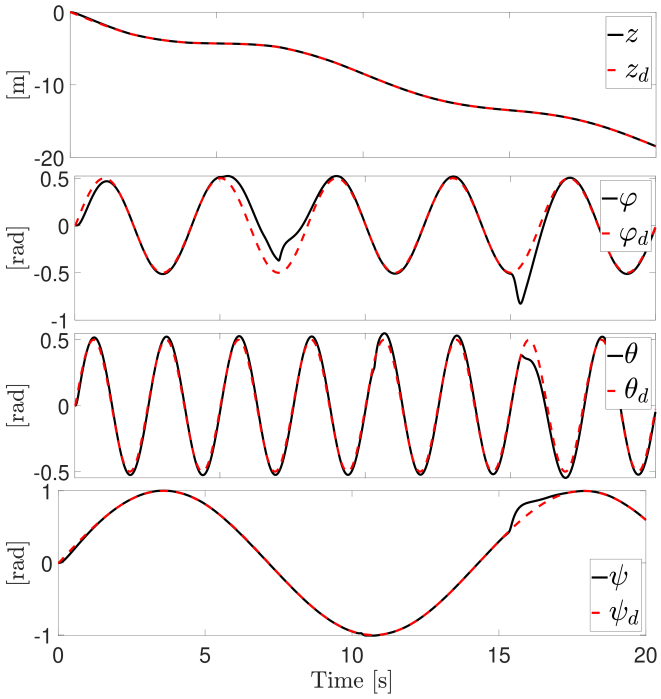


Fig. 5. Tracking performances.

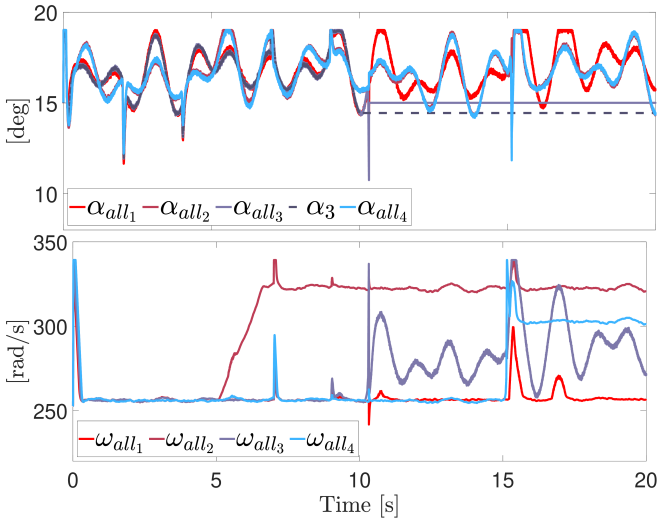


Fig. 6. Control inputs.

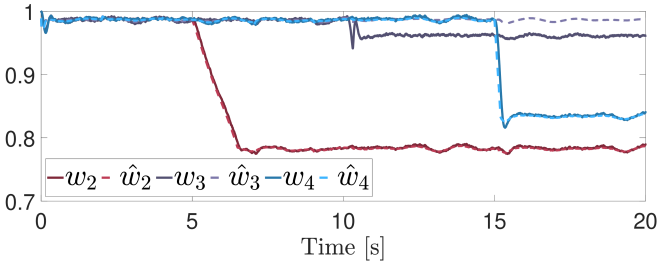


Fig. 7. Loss of effectiveness and its estimation.

the number of flights correctly executed without crash. The servo failure seems to be less critical than abrupt LOE: the FTC scheme manages positively 48 cases, while the remaining ones are detected but they are tackled too late for the vehicle to recover. If the pitch failure detection

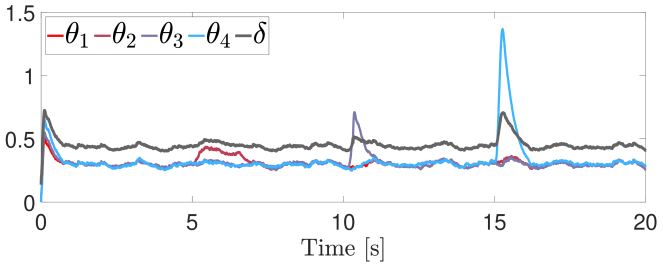


Fig. 8. Residual evaluation.

is disabled (i.e., the adaptation using $\hat{w}$ is active, while no stuck detection is performed), 17 flights are completed successfully because $\hat{w}$ alone is sufficient to avoid a crash, but the system shows a degradation of performances. In case of abrupt LOE, 42 scenarios are managed positively by the proposed scheme, while in absence of adaptation all of the flights fail. This means that the control law itself cannot withstand abrupt thrust losses (up to 40% of the lift force when the fault occurs) in such aggressive maneuvering.

Table 2. Success rate in presence and in absence of FTC

| | FTC | non FTC |
|---|---|---|
| Servo failure | 48/50 | 17/50 |
| Abrupt LOE | 42/50 | 0/50 |

## 6. CONCLUSION

We have proposed a control scheme for variable pitch quadrotors to cope with two kinds of actuator faults that affect the same input channel: pitch lock-in-place and rotor LOE. We have used AFD to determine the nature of the fault and then to eventually command a control reconfiguration that involves only the control allocation level. Simulation results show the severe consequences of such actuator faults if not tackled, as well as the effectiveness of the proposed solution. As a future work, we are experimentally investigating whether the following approach can cope with a bent or chipped propeller, which is a common damage in real flights. We are also developing a variable time interval to shorten the AFD in case of LOE, in order to increase the success rate in presence of abrupt LOE.

## REFERENCES

Arellano-Quintana, V.M., Merchán-Cruz, E.A., and Franchi, A. (2018). A novel experimental model and a drag-optimal allocation method for variable-pitch propellers in multirotors. *IEEE Access*, 6, 68155–68168.

Baldini, A., Felicetti, R., Freddi, A., Longhi, S., and Monteriù, A. (2019a). Octarotor fault tolerant control via dynamic surface control. In *2019 18th European Control Conference (ECC)*, 3892–3897. IEEE.

Baldini, A., Felicetti, R., Freddi, A., Longhi, S., Monteriù, A., and Rigatos, G. (2019b). Actuator fault tolerant position control of a quadrotor unmanned aerial vehicle. In *2019 4th Conference on Control and Fault Tolerant Systems (SysTol)*, 74–79. IEEE.

Chen, W.H., Yang, J., Guo, L., and Li, S. (2016). Disturbance-observer-based control and related methods - an overview. *IEEE Transactions on Industrial Electronics*, 63(2), 1083–1095.

Cutler, M. and How, J. (2012). Actuator constrained trajectory generation and control for variable-pitch quadrotors. In *AIAA Guidance, Navigation, and Control Conference*, 1–15.

Cutler, M. and How, J. (2015). Analysis and control of a variable-pitch quadrotor for agile flight. *Journal of Dynamic Systems, Measurement, and Control*, 137(10), 1–14.

Cutler, M., Ure, N.K., Michini, B., and How, J. (2011). Comparison of fixed and variable pitch actuators for agile quadrotors. In *AIAA Guidance, Navigation, and Control Conference*, 1–17.

Fresk, E. and Nikolakopoulos, G. (2014). Experimental model derivation and control of a variable pitch propeller equipped quadrotor. In *IEEE Conference on Control Applications (CCA)*, 723–729.

Gao, Z., Cecati, C., and Ding, S.X. (2015). A survey of fault diagnosis and fault-tolerant techniques—part ii: Fault diagnosis with knowledge-based and hybrid/active approaches. *IEEE Transactions on Industrial Electronics*, 62(6), 3768–3774.

Gupta, N., Kothari, M., and Abhishek (2016). Flight dynamics and nonlinear control design for variable-pitch quadrotors. In *IEEE American Control Conference (ACC)*, 3150–3155.

Harkegard, O. (2002). Efficient active set algorithms for solving constrained least squares problems in aircraft control allocation. In *41st IEEE Conference on Decision and Control*, volume 2, 1295–1300.

Hecker, S., Varga, A., and Ossmann, D. (2011). Diagnosis of actuator faults using lpv-gain scheduling techniques. In *AIAA Guidance, Navigation, and Control Conference*, 1–18.

Isermann, R. (2006). *Fault-diagnosis systems: an introduction from fault detection to fault tolerance*. Springer Science & Business Media.

Lanzon, A., Freddi, A., and Longhi, S. (2014). Flight control of a quadrotor vehicle subsequent to a rotor failure. *Journal of Guidance, Control, and Dynamics*, 37(2), 580–591.

Leishman, G.J. (2006). *Principles of helicopter aerodynamics with CD extra*. Cambridge university press.

Mancini, A., Caponetti, F., Monteriù, A., Frontoni, E., Zingaretti, P., and Longhi, S. (2007). Safe flying for an uav helicopter. In *Mediterranean Conference on Control Automation*, 1–6.

Pang, T., Peng, K., Lin, F., and Chen, B.M. (2016). Towards long-endurance flight: Design and implementation of a variable-pitch gasoline-engine quadrotor. In *12th IEEE International Conference on Control and Automation (ICCA)*, 767–772.

Podhradskỳ, M., Bone, J., Coopmans, C., and Jensen, A. (2013). Battery model-based thrust controller for a small, low cost multirotor unmanned aerial vehicles. In *2013 International Conference on Unmanned Aircraft Systems (ICUAS)*, 105–113. IEEE.

Porter, R., Shirinzadeh, B., and Choi, M.H. (2016). Experimental analysis of variable collective-pitch rotor systems for multirotor helicopter applications. *Journal of Intelligent & Robotic Systems*, 83(2), 271–288.

Pretorius, A. and Boje, E. (2014). Design and modelling of a quadrotor helicopter with variable pitch rotors for aggressive manoeuvres. *IFAC Proceedings Volumes*, 47(3), 12208–12213.

Punčochář, I. and Škach, J. (2018). A survey of active fault diagnosis methods. *IFAC-PapersOnLine*, 51(24), 1091–1098.

Qiao, G., Liu, G., Shi, Z., Wang, Y., Ma, S., and Lim, T.C. (2018). A review of electromechanical actuators for more/all electric aircraft systems. *Proceedings of the Institution of Mechanical Engineers, Part C: Journal of Mechanical Engineering Science*, 232(22), 4128–4151.

Sheng, S. and Sun, C. (2016). Control and optimization of a variable-pitch quadrotor with minimum power consumption. *Energies*, 9(4), 232.

TDK InvenSense (2016). Mpu-9250, nine-axis (gyro+ accelerometer+ compass) mems motiontracking™ device. `https://invensense.tdk.com/download-pdf/mpu-9250-datasheet/`.

Zhou, Q.L., Zhang, Y., Rabbath, C.A., and Theilliol, D. (2010). Design of feedback linearization control and reconfigurable control allocation with application to a quadrotor uav. In *2010 Conference on Control and Fault-Tolerant Systems (SysTol)*, 371–376. IEEE.